Experimental and theoretical investigation of the lateral Casimir force between corrugated surfaces

F. Chen and U. Mohideen*
Department of Physics, University of California, Riverside, California 92521

G. L. Klimchitskaya† and V. M. Mostepanenko‡
Departamento de Física, Universidade Federal da Paraíba, C.P. 5008, CEP 58059-970, João Pessoa, Pb-Brazil
(Received 31 May 2002; revised manuscript received 12 July 2002; published 25 September 2002)

The lateral Casimir force acting between a sinusoidally corrugated gold plate and sphere was calculated and measured. The experimental setup was based on the atomic force microscope specially adapted for the measurement of the lateral Casimir force. The measured force oscillates sinusoidally as a function of the phase difference between the two corrugations. Both systematic and random errors are analyzed and a lateral force amplitude of 3.2×10^{-13} N was measured at a separation distance of 221 nm with a resulting relative error 24% at a 95% confidence probability. The dependence of the measured lateral force amplitude on separation was investigated and shown to be consistent with the inverse fourth power distance dependence. The complete theory of the lateral Casimir force is presented including finite conductivity and roughness corrections. The obtained theoretical dependence was analyzed as a function of surface separation, corrugation amplitudes, phase difference, and plasma wavelength of a metal. The theory was compared with the experimental data and shown to be in good agreement. The constraints on hypothetical Yukawa-type interactions following from the measurements of the lateral Casimir force are calculated. The possible applications of the lateral vacuum forces to nanotechnology are discussed.

DOI: 10.1103/PhysRevA.66.032113 PACS number(s): 12.20.Fv, 42.50.Lc

I. INTRODUCTION

It is well known that the existence of zero-point electromagnetic oscillations leads to the Casimir force acting normal to neutral and parallel metal plates placed in vacuum [1]. This is a purely quantum effect caused by the alteration of the zero-point oscillation spectrum of a quantized electromagnetic field by the metallic boundaries (see the monographs [2–4] and references therein). Recently, the normal Casimir force acting perpendicular to the two surfaces has attracted much experimental and theoretical attention. It was measured between a flat plate and a spherical lens by means of a torsion pendulum [5] and between two parallel plates using a tunneling electromechanical transducer [6]. The highest precision was achieved in the experimenatal research of the normal Casimir force between a sphere and a flat plate by means of the atomic force microscope (AFM) [7–10]. In the case of the plate with periodic uniaxial sinusoidal corrugations and sphere the nontrivial boundary dependence of the normal Casimir force was demonstrated [11]. These experimental achievements have stimulated an extensive theoretical study of various corrections to the Casimir force. Here the finite conductivity corrections to the normal Casimir force due to the boundary metal were investigated in detail [12–14]. The other influential factor that may contribute considerably to the normal Casimir force at small separations is surface roughness [8,15–17]. In Refs. [18–24] the thermal corrections were investigated in the case of real metals which are significant at separations larger than $1\,\mu$m. Also, the combined effect of different corrections was examined (for a recent review of the subject see Ref. [25]).

There is an important need for further research on the Casimir effect motivated by the fact that it is finding new applications in both fundamental science and engineering. Thus, in the framework of modern unified theories, involving compact extra dimensions and light elementary particles, precision measurements of the Casimir force have been used to set limits on the presence of hypothetical forces [26–31]. Technologically, both static and dynamic micromachines actuated by the normal Casimir force have recently been demonstrated [32,33]. It was also shown that the adhesion and sticking of moving parts in micromachines is due to the Casimir effect [34].

Similar to the normal Casimir force, the lateral Casimir force may exist when the bodies are asymmetrically positioned or their properties are anisotropic. The existence of the lateral Casimir force opens new opportunities for the application of the Casimir force in micromachines. The lateral Casimir force also originates from the modification of electromagnetic zero-point oscillations by material boundaries. The possibility of a lateral Casimir force for anisotropic boundaries was investigated theoretically and a harmonic dependence on a corresponding angle was predicted [3,35,36]. For two aligned corrugated plates made of ideal metal the lateral Casimir force was discussed in [37–39] and a harmonic dependence of the result on a phase shift between corrugations was found. Note that other motional frictional forces between two flat parallel surfaces have been suggested but they would be several orders of magnitude smaller [40,41].

In Ref. [42] the first measurement of the lateral Casimir

*Email address: umar.mohideen@ucr.edu
†On leave from North-West Polytechnical University, St. Petersburg, Russia. Email address: galina@fisica.ufpb.br
‡On leave from Research and Innovation Enterprise "Modus," Moscow, Russia. Email address: mostep@fisica.ufpb.br

force was reported and the theoretical expression for it was obtained in the case of real metals of finite conductivity. This force acts between an aligned corrugated sphere and a plate in a direction tangential to the corrugated surfaces. The predicted sinusoidal dependence of the lateral force on the phase shift between corrugations was confirmed.

In this paper we present the detailed experimental and theoretical investigation of the lateral Casimir force acting between a corrugated sphere situated near a corrugated plate with aligned sinusoidal corrugations. The theoretical dependence for the lateral force is analyzed and the optimum values of the parameters leading to the maximum values of the lateral force are found. It is shown that even a small misalignment of the corrugation axes will quench the lateral Casimir force to zero. The effect of surface roughness is estimated and shown to be insignificant. Experimentally, new measurement data are presented and the calibration procedures by means of the normal and lateral electric forces are discussed. The systematic and random errors are analyzed and the agreement between theory and experiment is confirmed with good precision. The lateral hypothetical force that may originate from extra dimensions or from exchange of light elementary particles is then calculated and the constraints on its parameters are obtained.

The paper is organized as follows. In Sec. II the theory is developed describing the lateral Casimir force for the configuration of a metallized sphere and a plate with the uniaxial corrugations taking into account the finite conductivity and roughness corrections. In Sec. III the experimental setup is described. Section IV contains the measurement scheme including calibration procedures. In Sec. V the obtained data are presented together with the error analyses and comparison of the experimental results to the theory. In Sec. VI the new constraints on the parameters of hypothetical interactions are found. Section VII contains conclusions and discussion.

II. CALCULATION OF THE LATERAL CASIMIR FORCE BETWEEN SURFACES WITH UNIAXIAL CORRUGATIONS

It is well known that the regularized zero-point energy per unit area for two parallel plates of infinite conductivity a distance z apart is given by [1–4,25]

$$E_{pp}^{(0)}(z)=-\frac{\pi^2}{720}\frac{\hbar c}{z^3}. \tag{1}$$

This results in the normal Casimir force per unit area

$$F_{pp}^{(0)}(z)=-\frac{\partial E_{pp}^{(0)}(z)}{\partial z}=-\frac{\pi^2}{240}\frac{\hbar c}{z^4}, \tag{2}$$

which acts perpendicular to the surface of the plates.

As real metals have only a finite conductivity, corresponding corrections to Eqs. (1) and (2) can be incorporated in terms of the plasma wavelength λ_p. This was first done in [43–45] up to the first perturbation order and in [46] up to the second order of a small parameter $\lambda_p/(2\pi z)$. To get the

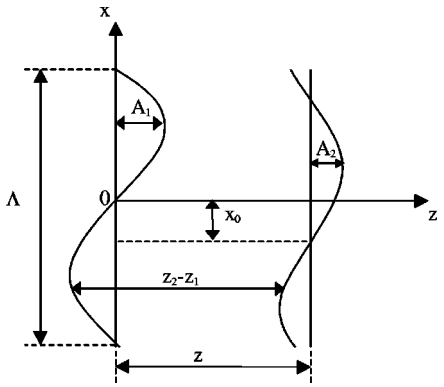

FIG. 1. Configuration of two parallel plates with uniaxial sinusoidal corrugations of equal periods.

results applicable at the separations $z \geqslant \lambda_p$ with an error of about 1% to 2%, that are required below, we use the perturbation expansion up to the fourth order obtained in [12] (see also [24,25,47]):

$$E_{pp}(z)=-\frac{\pi^2\hbar c}{720z^3}\left[1+\sum_{n=1}^{4}c_n\left(\frac{\lambda_p}{2\pi z}\right)^n\right], \tag{3}$$

where the coefficients are

$$c_1=-4,\ c_2=72/5,\ c_3=-\frac{320}{7}\left(1-\frac{\pi^2}{210}\right),$$

$$c_4=\frac{400}{3}\left(1-\frac{163\pi^2}{7350}\right). \tag{4}$$

For flat plates at rest, the lateral Casimir force projection is absent. If, however, the rotational symmetry against the axis perpendicular to the plates is broken than the lateral projection of the Casimir force may appear [3,35–39]. As the first example, let us consider plates covered by the longitudinal uniaxial corrugations of equal periods described by the functions

$$z_1=A_1\sin(2\pi x/\Lambda),$$

$$z_2=z+A_2\sin(2\pi x/\Lambda+\varphi), \tag{5}$$

where z is the mean separation distance between the two surfaces, Λ is the corrugation period, $A_{1,2}$ are the corrugation amplitudes, and $\varphi \equiv 2\pi x_0/\Lambda$ is the phase shift (see Fig. 1).

The normal separation distance between two opposite points of the corrugated surfaces given by Eq. (5) is

$$z_2-z_1=z+A_2\sin(2\pi x/\Lambda+\varphi)-A_1\sin(2\pi x/\Lambda). \tag{6}$$

By simple transformations it can be identically represented as

$$z_2-z_1=z+b\cos(2\pi x/\Lambda-\alpha), \tag{7}$$

where the following notations are introduced

$$b=b(\varphi)=(A_1^2+A_2^2-2A_1A_2\cos\varphi)^{1/2},$$

$$\tan\alpha=(A_2\cos\varphi-A_1)/(A_2\sin\varphi). \tag{8}$$

The representation of the separation distance in the form of Eqs. (7) and (8) is convenient for the calculation of the Casimir energy per unit area between the corrugated plates. It can be found by additive summation of the results obtained for plane plates [see Eq. (3)]. In doing so we assume that all separation distances z_2-z_1 given by Eq. (7) are equally probable. This approximation has been successfully applied in many calculations of the Casimir effect in configurations where the variables are not separable and the exact Green's function of the wave equation cannot be found explicitly (see, e.g., [2,3,8,11,15,16,25]). As was shown in Ref. [39] the additive summation works well for corrugated plates with a large corrugation period, e.g., with $\Lambda>z$, which is the case in our experiment (see Sec. III). As a result, the Casimir energy density between corrugated plates is given by

$$E_{pp}^{cor}(z,\varphi)=\frac{1}{\Lambda}\int_0^{\Lambda}E_{pp}(z_2-z_1)dx, \tag{9}$$

where z_2-z_1 is defined by Eqs. (7) and (8). Substituting Eqs. (7) and (8) into Eq. (3) and integrating, one obtains

$$E_{pp}^{cor}(z,\varphi)=-\frac{\pi^2\hbar c}{720z^3}\sum_{n=0}^{4}c_n\left(\frac{\lambda_p}{2\pi z}\right)^n X_n(\beta), \tag{10}$$

where $\beta\equiv b(\varphi)/z$, c_n are defined in Eq. (4), and the following notations are used

$$X_0(\beta)=\frac{2+\beta^2}{2(1-\beta^2)^{5/2}},\quad X_1(\beta)=\frac{2+3\beta^2}{2(1-\beta^2)^{7/2}},$$

$$X_2(\beta)=\frac{8+24\beta^2+3\beta^4}{8(1-\beta^2)^{9/2}},\quad X_3(\beta)=\frac{8+40\beta^2+15\beta^4}{8(1-\beta^2)^{11/2}},$$

$$X_4(\beta)=\frac{16+120\beta^2+90\beta^4+5\beta^6}{16(1-\beta^2)^{13/2}}. \tag{11}$$

Experimentally it is hard to maintain two parallel plates uniformly separated by distances less than a micron. So one of the plates is usually replaced by a metallized sphere or a spherical lens of large radius $R\gg z$ [5,7–11,32,33]. In the experiments described below (see Secs. III–V) a sphere imprinted with sinusoidal corrugations was used instead of one of the corrugated plates. For such a configuration the normal Casimir force can be calculated approximately by the use of proximity force theorem (PFT) [48] as

$$F^{nor}(z,\varphi)=2\pi RE_{pp}^{cor}(z,\varphi), \tag{12}$$

where the energy per unit area for the configuration of two corrugated plates is given by the right-hand side of Eq. (10). For our experimental parameters, the two conditions $z\ll R$ and $\Lambda\ll R$ are fulfilled. As a result the error introduced by the PFT in the configuration under consideration is of order 0.2% [49,50], which is acceptable for the goals of this paper.

By integrating the normal force (12) with respect to the surface separation, the energy of a corrugated sphere and a plate is obtained. Then, differentiating with respect to the phase shift, one finds the lateral Casimir force

$$F^{lat}(z,\varphi)=-\frac{2\pi}{\Lambda}\frac{\partial}{\partial\varphi}\int_z^{\infty}dyF^{nor}(y,\varphi). \tag{13}$$

Substituting Eqs. (10)–(12) into Eq. (13) we finally obtain after integration and differentiation

$$F^{lat}(z,\varphi)=\frac{\pi^4R\hbar c}{120z^4}\frac{A_1A_2\sin\varphi}{\Lambda(1-\beta^2)^{5/2}}\left[1+\sum_{n=1}^{4}c_{n,x}\left(\frac{\lambda_p}{2\pi z}\right)^n\right], \tag{14}$$

where β was defined after Eq. (10) and the expansion coefficients are given by

$$c_{1,x}=\frac{4+\beta^2}{3(1-\beta^2)}c_1,\quad c_{2,x}=\frac{5(4+3\beta^2)}{12(1-\beta^2)^2}c_2, \tag{15}$$

$$c_{3,x}=\frac{8+12\beta^2+\beta^4}{4(1-\beta^2)^3}c_3,\quad c_{4,x}=\frac{7(8+20\beta^2+5\beta^4)}{24(1-\beta^2)^4}c_4.$$

The above Eqs. (14) and (15) give us the expression for the lateral Casimir force for the configuration of a corrugated sphere and a plate including the finite conductivity corrections. There are also corrections to Eqs. (14) and (15) due to nonzero temperature. However, at separations smaller than 0.5 μm considered in Secs. III–V they contribute much less than 1% [18–25] and thereby can be neglected. Another factor that could contribute to the lateral Casimir force is surface roughness. It was shown to lead to rather large contributions to the normal Casimir force at separations below 1 μm [15–17,25]. Because of this, the effect of surface roughness on the lateral Casimir force should be considered in more detail.

There are two kinds of surface roughness on the metal surfaces: infrequently distributed tall crystals and short-scale stochastic distortions. The infrequent tall crystals practically do not influence the lateral Casimir force as they are situated nonperiodically and lead to zero contribution after the averaging over the corrugation period. The situation here is the same as for two corrugated plates with different corrugation periods. In Ref. [15] it was shown that if the corrugation periods are different (and larger than a separation distance z) the Casimir energy does not depend on a lateral shift of one plate relative to the other one. As a result, the derivative of the energy with respect to the phase shift is equal to zero and the lateral force is absent.

To take stochastic roughness into account we can change $F^{lat}(z,\varphi)$ for $F^{lat}(z_i,\varphi)$ with

$$z_i=z+x_i,\quad \langle x_i\rangle=0,\quad \langle x_i^2\rangle=\frac{1}{2}A_{st}^2, \tag{16}$$

where x_i describes the random change of the separation distance due to the stochastic roughness with an amplitude A_{st},

and the angle brackets denote the averaging over the ensemble of all particular realizations of the corresponding stochastic function. It is important to note that z_i enters Eq. (14) directly as a replacement for z and indirectly through the functions of β^2 that should now be changed to $\beta_i^2=b^2/(z+x_i)^2$. The lateral Casimir force with account of stochastic roughness is defined as

$$F_{st}^{lat}(z,\varphi)=\langle F^{lat}(z_i,\varphi)\rangle. \tag{17}$$

Performing the computations up to the second order in powers of A_{st}/z the following result is obtained:

$$F_{st}^{lat}(z,\varphi)=\frac{\pi^4 R\hbar c}{120z^4}\,\frac{A_1A_2\sin\varphi}{\Lambda(1-\beta^2)^{5/2}} \times\left[1+\frac{5(1+9\beta^2-3\beta^4)}{4(1-\beta^2)^2}\,\frac{A_{st}^2}{z^2}\right] \times\left[1+\sum_{n=1}^{4}c_{n,x}^{st}\left(\frac{\lambda_p}{2\pi z}\right)^n\right]. \tag{18}$$

Here the coefficients $c_{n,x}^{st}$ are only slightly different from those given by Eq. (15) (which does not include stochastic roughness). For example, for $n=1$, 2 their expressions are

$$c_{1,x}^{st}=c_{1,x}\left[1+\frac{15\beta^2}{2(4+\beta^2)(1-\beta^2)}\,\frac{A_{st}^2}{z^2}\right],$$

$$c_{2,x}^{st}=c_{2,x}\left[1+\frac{3\beta^2(11+3\beta^2)}{2(4+\beta^2)(1-\beta^2)}\,\frac{A_{st}^2}{z^2}\right]. \tag{19}$$

If we take into consideration the typical values of $\beta^2<0.1$ and $A_{st}\approx 10$ nm, Eq. (18) can be approximately rewritten in a more simple form,

$$F_{st}^{lat}(z,\varphi)\approx F^{lat}(z,\varphi)\left[1+\frac{5(1+9\beta^2-3\beta^4)}{4(1-\beta^2)^2}\,\frac{A_{st}^2}{z^2}\right]. \tag{20}$$

From Eq. (20) one can conclude that at separations $z>200$ nm used in the experiment the influence of stochastic roughness on the lateral force is less than 1% and can be neglected. Thus Eqs. (14) and (15) give us a reliable theoretical expression for the lateral Casimir force including all necessary corrections.

The most interesting characteristic feature of Eq. (14) is the harmonic dependence of the lateral Casimir force on a phase shift between the corrugations of both bodies. However, the actual dependence of F^{lat} on φ is not exactly sinusoidal because β also depends on φ which leads to some deviation from the exact sine. To illustrate this, in Fig. 2 the dependence of F^{lat}/F_{max}^{lat} on φ at a separation $z=272$ nm is plotted (solid line). In the same figure the graph of $\sin\varphi$ is shown by a dashed line. To make deviations from a perfect sine larger, the case of equal amplitudes $A_1=A_2=59$ nm is considered (in the experiment of Secs. III–V the amplitude

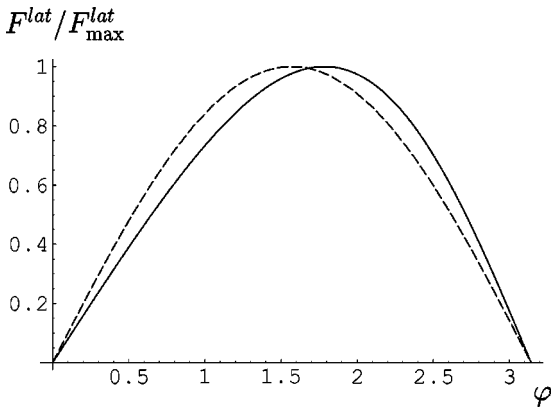

FIG. 2. The lateral Casimir force between the corrugated plate and sphere normalized for its maximum value as a function of a phase shift (solid line) is compared to a graph of sine (dashed line).

of corrugations on a sphere is smaller than on the plate). As is seen from Fig. 2, the maximum of the lateral Casimir force is displaced from the position of the maximum of sine by approximately 0.21 rad.

The values of the lateral force given by Eq. (14) depend on the corrugation amplitudes (both in an explicit form and through the parameter b). In Fig. 3 the graph of F_{max}^{lat} as a function of A_2 is plotted for $A_1=59$ nm. For each value of A_2 the distance $z=z_0+A_1+A_2$ is chosen where $z_0=154$ nm which is in accordance with the experimental value of the separation on contact (see Secs. III–V). It is seen that F_{max}^{lat} increases with an increase of A_2 and takes the largest value $F_{max}^{lat}=1.2\times10^{-12}$ N when $A_2=A_1$.

The effects of the finite conductivity of the boundary metal make a significant contribution to the value of the lateral Casimir force from Eq. (14). This is illustrated by Fig. 4, where the correction coefficient $\eta=F^{lat}/F_0^{lat}$ is plotted as a function of separation distance, and F_0^{lat} is computed for an ideal metal (i.e., with $\lambda_p=0$). Here the experimental values of the corrugation amplitudes were chosen, i.e., $A_1=59$ nm, $A_2=8$ nm, and a phase shift $\varphi=\pi/2$ (see Secs. III–V). It should be noted that the value of the correction factor η depends only slightly on the phase shift. The value

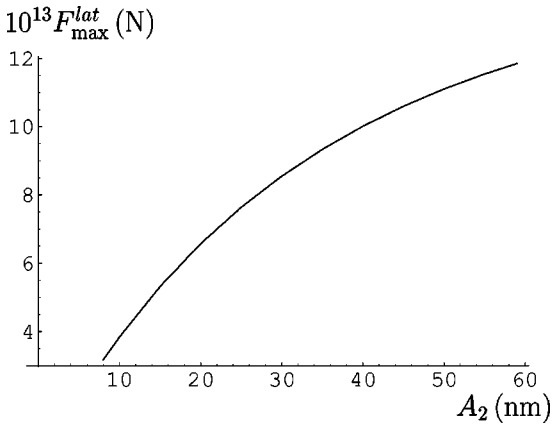

FIG. 3. The maximum value of the lateral Casimir force as a function of a corrugation amplitude on a sphere.

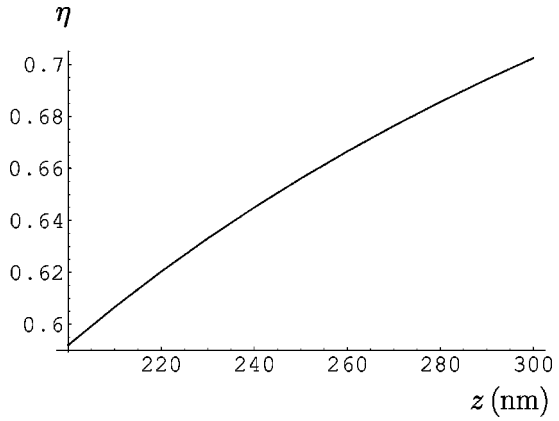

FIG. 4. Correction coefficient due to the effects of finite conductivity on the lateral Casimir force between the corrugated plate and sphere made of ideal metals as a function of surface separation.

of the plasma wavelength $\lambda_p = 136$ nm for Au was used [13]. It is seen from the figure that in the separation range of interest here the correction coefficient changes between 0.6 and 0.7. Because of this, it would be incorrect to use a theory which does not include the effect of the finite conductivity corrections for interpretation of the experimental data on the lateral Casimir force.

At the end of this section we briefly discuss the demand that the corrugations be uniaxial. This demand is of crucial importance for the observation of the lateral Casimir force. In fact, let us assume for a moment that there is some nonzero angle ϑ between the corrugation axes. Then the phase shift φ along the x axis becomes the periodical function of y with a period $\Lambda_y = \Lambda \cot \vartheta$. In the limit of one period $\varphi(y)$ depends on y linearly, taking on values from 0 to 2π. To obtain the resulting lateral force, the expression $F^{lat}[z, \varphi(y)]$ should be averaged over the period Λ_y which leads to a zero value. For real bodies of finite size the lateral Casimir force will exist only for small deviations of the corrugation axes from parallelity such that $\Lambda \cot \vartheta$ is much larger than the smallest body. In our case the smallest body is the 10-μm section of the sphere covered with corrugations. That is why in order to observe the lateral Casimir force one must make sure that the angle between the corrugation axes is bounded by the condition $\vartheta \ll 0.1$ rad.

III. EXPERIMENTAL SETUP

A schematic diagram of the experiment is shown in Fig. 5. These experiments are performed using a standard AFM at a pressure below 50 mTorr and at room temperature. The experiment requires two sinusoidally corrugated surfaces with their respective axes perfectly parallel. Misalignment by 3° of the corrugation axes can lead to loss of any lateral force due to the crossover of the axes as is described in Sec. II. A plastic diffraction grating with uniaxial sinusoidal corrugations of period $\Lambda = 1.2$ μm and an amplitude of 90 nm was used as the corrugated plate. In order to obtain perfect orientation and phase between the two corrugated surfaces a special *in situ* procedure was developed, where the corrugations

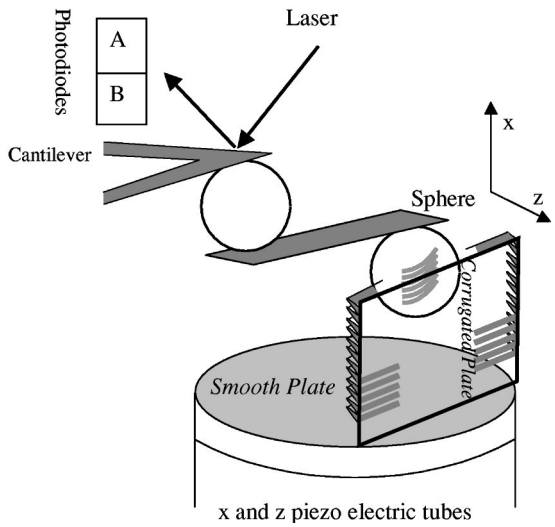

FIG. 5. Schematic of experimental setup. For clarity, the sizes of the corrugations have been exaggerated. The *x*-piezo and *z*-piezo are independent.

from the plate are imprinted on the gold coated sphere by pressure. This imprinting procedure required special adaptation of the cantilever which is described next.

A polystyrene sphere was attached to the tip of a 320 μm long cantilever with conductive silver epoxy. After this a <10 μm thick, 100–200 μm wide, and 0.5 mm long piece of freshly cleaved mica was attached to the bottom of the sphere with silver epoxy. Then a second polystyrene sphere of $2R = 200 \pm 4$ μm diameter was mounted on the tip of mica with the same silver epoxy. This second sphere is imprinted with the corrugations and will interact with the corrugated plate. The sphere and the plates are mounted as shown in Fig. 5. Let us first note that the laser beam for the detection of the cantilever deflection is reflected off its tip. The addition of the first sphere and mica plate is needed to isolate the laser reflection spot on the cantilever tip from the interaction region between the two corrugated surfaces. This isolation is necessary to reduce the effect of scattered light from the top and sides of the corrugated plate. Second, the procedure developed for the imprinting of the corrugations requires access to interior regions of the corrugated plate, far away from the edges. Third, the addition of the mica plate leads also to an effective increase in the detection sensitivity due to the increase in the lever arm. The cantilever (with mica plate and spheres), corrugated plate, and a smooth flat plate (polished sapphire) were then coated with about 400 nm of gold in a thermal evaporator. A small region close to one edge of the corrugated plate is also coated with 100 nm of aluminum. As Al exhibits more hardness than gold, this region is used to imprint the corrugations from the plate onto the gold coated sphere.

The cantilever (with mica plate and spheres), corrugated plate, and a smooth flat plate are then mounted as shown in Fig. 5. Now, the imprinting of the corrugations on the sphere is done. The sphere is moved over to the region of the corrugated plate coated with Al. The other side of the sphere is mechanically supported and the corrugations are imprinted on the gold coating of the surface by pressure using the piezos shown. A scanning electron micrograph of the imprint

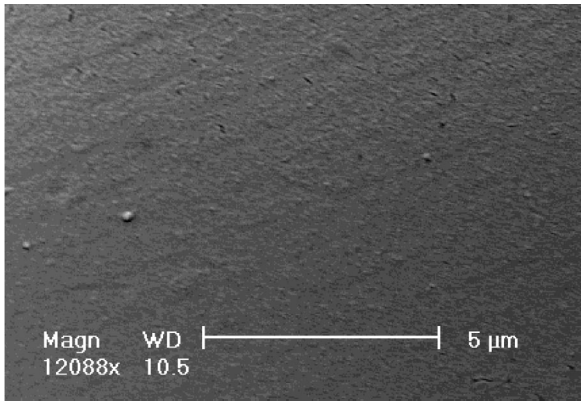

FIG. 6. Scanning electron micrograph of the imprint of the corrugations on the sphere.

on the sphere, taken after the completion of the experiment, is shown in Fig. 6. An AFM scan of the imprinted corrugations is shown in Fig. 7. The amplitude of the imprinted corrugations is measured from the AFM scan to be $A_2=8\pm1$ nm. The amplitude of the corrugations on the metallized plate was also measured, using the AFM, $A_1=59\pm7$ nm. These AFM measurements were made after completion of all the lateral force experiments which are reported below. After this imprinting, the mechanical supports are removed and the sphere is translated over to the gold coated area of the plate. Extreme care to preserve the parallel orientation of the two corrugations is necessary during this translation, as any misallignment leads to the destruction of any lateral Casimir force. This is done by tracking the orientation of the cantilever during this translation by reflecting two optical beams from the edges of the cantilever holder. The reflected beam positions allow measurement of the cantilever orientation to an accuracy of 2×10^{-3} rad.

The corrugated plate is mounted on two piezoelectric tubes that allow independent movement of the plate in the vertical and the horizontal directions with the help of a *x*-piezo and a *z*-piezo, respectively. Movement in the *x* direction with the *x*-piezo is necessary to achieve lateral phase shift φ between the corrugated sphere and the plate. Independent movement in the *z* direction is necessary for control of the surface separation between the corrugated sphere and plate. The corrugated plate is mounted vertically in order to increase the sensitivity for detection of lateral forces and suppress the effect of the normal Casimir force on the cantilever. Thus a lateral force tangential to the corrugated sphere surface would result in the usual bending of the cantilever in response to the force. Whereas a force acting normal to the sphere and corrugated plate (from the normal Casimir force) would lead to the torsional deflection (rotation) of the cantilever. The torsional spring constant of this cantilever k_{tor} is much greater than the bending spring constant k_{ben}, making it much more sensitive to detecting the lateral Casimir force, while simultaneously suppressing the effect of the normal Casimir force.

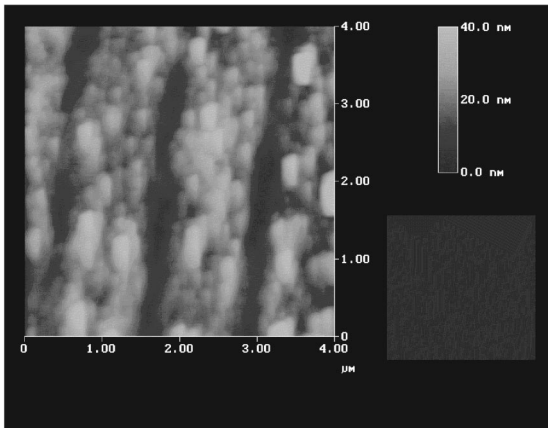

FIG. 7. Atomic force microscope scan of the imprinted corrugations on the sphere.

IV. MEASUREMENT SCHEME

The calibration of the cantilever (k_{tor} and k_{ben}) and the measurement of the residual potentials between the sphere and plate is done by electrostatic means [7–11]. These calibrations are done after the measurement of the lateral Casimir forces, but is reported in this section for the benefit of continuity. Here, in order to measure k_{tor}, the sphere is kept grounded and various voltages are applied to the corrugated plate. The normal electrostatic force between the corrugated sphere and plate is given by

$$F_z^{el}(z,\varphi)=-\pi R\varepsilon_0\frac{(V_1-V_0)^2}{z}\frac{1}{\sqrt{1-\beta^2}}, \qquad (21)$$

where ε_0 is the permittivity of free space. V_1 are the voltages applied on the corrugated plate and V_0 is the residual potential on the grounded sphere. The approximate expression (21) was obtained by exactly the same procedure as Eq. (12) for the normal Casimir force [instead of Eq. (3), we have started here from the energy per unit area of a capacitor formed by two large, flat conducting sheets].

If V_1 is applied to the corrugated plate, the electrostatic force acting normal to the spherical surface leads to the torsional rotation of the cantilever. By applying different V_1 we can solve for the torsional spring constant $k_{tor}=0.138\pm0.005$ N/m and the residual voltage between the sphere and the corrugated plate $V_0=-0.135$ V. Next the measurement of k_{ben} is done. The sphere is moved away from the vertical corrugated plate and brought closer to the smooth plate which is positioned horizontally at the bottom as shown in Fig. 5. Again different voltages V_1 are applied to the bottom plate [here in Eq. (21) $A_1=A_2=\beta=0$ due to the smooth surfaces], and the electrostatic force leads to the normal bending of the cantilever. We again solve for the normal spring constant $k_{ben}=0.0052\pm0.0001$ N/m and the residual voltage between the sphere and the smooth plate. Note that $k_{tor}\gg k_{ben}$ is required for isolation and detection of the role of the lateral Casimir force. The piezoextension in the *x* direction with applied voltage was calibrated by optical interferometry [51]. The horizontal displacement of the piezo in the *z* direction was calibrated with AFM standards.

Similar to the lateral Casimir force, there also exists a lateral electrostatic force which arises from the presence of an applied or residual electrostatic potential difference between the two corrugated surfaces. It is given by

$$F_x^{el}(z,\varphi)=2\pi^2 R\varepsilon_0(V_1-V_0)^2\frac{A_1A_2}{\Lambda z^2}$$

$$\times\frac{\sin\varphi}{\sqrt{1-\beta^2}(1+\sqrt{1-\beta^2})}. \qquad (22)$$

This expression is obtained from Eq. (21) by integration with respect to z (in order to find the electric energy in configuration of a corrugated plate and a corrugated sphere) and differentiation with respect to $x_0=\varphi\Lambda/2\pi$. Both Eqs. (21) and (22) are valid with an error smaller than 1% for the experimental parameters under consideration.

In contrast with the lateral Casimir force, the lateral electrostatic force is dependent on the inverse second power of the separation distance z between the corrugated surfaces (the dependence of β on z is small). One can measure the lateral electrostatic force in order to distinguish its differences from the lateral Casimir force. The measurement of the lateral electrostatic force also will help in providing an approximate measure of the separation distance between the two corrugated surfaces on contact. Note that because of the roughness of the metal surfaces and the imprinting procedure used, the contact separation is much greater than the distances between the means of the corrugations.

Two different voltage differences between the corrugated plate and sphere were used in the measurements of the lateral electrostatic force. In the first case, we utilized the residual voltage difference $V_0=0.135$ V with $V_1=0$ V. The sphere was moved next to the corrugated plate and the separation distance between the two surfaces was kept fixed. To measure the lateral electrostatic force F_x^{el} as a function of the phase φ, the corrugated plate is moved in the x direction by x-piezo in average steps of 0.46 nm (due to the small nonlinear response of the piezo, the exact step size will differ by a few percent depending on the applied voltage [51]) and the lateral electrostatic force is measured at each step. The corrugated plate could have been mounted with a small but nonzero tilt away from the vertical (x axis). Such tilts would lead to changes in surface separations during the above translations of the plate in the x direction. In order to rectify this, a small correction voltage is applied to the z-piezo, synchronous with the lateral translation in the x direction, to keep the surface separation distance between the corrugated sphere and plate constant. The lateral force measurement is repeated 60 times and the average lateral force at each step is recorded. The measured force in this case is actually the sum of the lateral Casimir force and the lateral electrostatic force. The observed lateral force is shown in Fig. 8. A sine curve is best fit to the observed data and an amplitude of 16.2×10^{-13} N is obtained for the total force. This amplitude when fit to the sum of the two lateral forces (Casimir +electrostatic) resulting from Eq. (14) and from Eq. (22) leads to a separation distance of $z=225\pm4$ nm between the two corrugated surfaces. This separation distance is used to subtract the lateral Casimir force from the measured total force to obtain the lateral electrostatic force. The error in the separation distance z corresponds to the error in the amplitude of the electrostatic force resulting from the 16 nm uncertainty in x. This uncertainty is x was determined experimentally by measuring the random variations in the phase of the peaks of the sinusoidal oscillations from 30 scans. Note that this random uncertainty in the phase corresponding to 16 nm is much smaller than the period of corrugations ($\Lambda=1.2$ μm). The separation between the sphere and corrugated plate is changed in steps of 24 nm and the measurement is repeated. This was repeated until the sphere and the corrugated plate come in contact. The surface separation on contact of the two corrugated surfaces is 202 ± 38 nm (the large uncertainty is the total of the uncertainty of 24 nm resulting from the step size, the 5 nm systematic uncertainty from the measurement of the force amplitude, and the 9 nm random error from the force measurement at different separation distances).

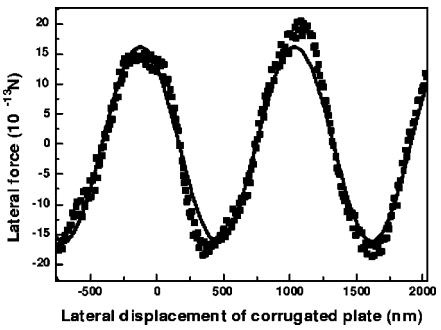

FIG. 8. The average measured sum of the electric and Casimir lateral forces as a function of the lateral displacement of the corrugated plate is shown as solid squares. The solid line is the best fit sine curve to the data leading to a lateral force amplitude of 16.2×10^{-13} N.

In the second case a different voltage $V_1=-0.055$ V is applied to the corrugated plate ($V_0=-0.135$ V) and the lateral electrostatic force measurement is repeated. Again the distance between the corrugated surfaces is changed in steps of 24 nm, starting at some separation, until the two surfaces come into contact. The separation between the two corrugated surfaces on contact was 169 ± 33 nm (in this case a 4 nm random error from the force measurement at different separations was present). Thus the average separation on contact from the two applied voltages was 186 ± 38 nm. Note that the lateral electrostatic force measurement was done a few hours after the measurement of the lateral Casimir force (described below) and thus this separation distance on contact obtained from the lateral electrostatic force serves as only a constraint on the separation distances between the corrugated surfaces to be expected for the measurement of the lateral Casimir force. In Fig. 9, a $\log_{10}$-$\log_{10}$ plot of the measured lateral electrostatic force amplitude as a function of the separation distance is done for the two applied voltages as solid squares and triangles, respectively. The slopes of the best straight fit lines (using the least-squares procedure) to the two sets of measured lateral

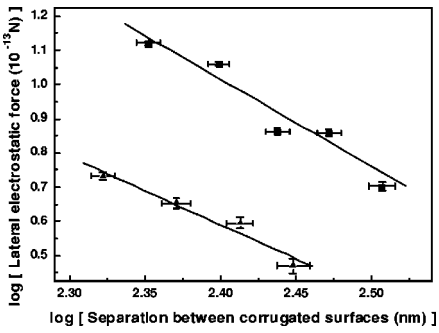

FIG. 9. The $\log_{10}$-$\log_{10}$ plot of the measured lateral electrostatic force amplitude as a function of the surface separation distance is shown as solid squares.

electrostatic forces are 2.5 ± 0.4 and 2.0 ± 0.3, respectively, leading to an average slope of 2.3 ± 0.4. Thus the measured slope is consistent with the second power distance dependence expected from Eq. (22).

V. OBTAINED DATA, ERROR ANALYSES, AND COMPARISON WITH THEORY

In this section we discuss the results obtained with the measurement of the lateral Casimir force. The measurement procedures described above with the measurement of the lateral electrostatic force are used. The important difference is that for the measurement of the lateral Casimir force, the residual potential difference between the corrugated sphere and plate is compensated by application of voltage V_0 to the corrugated plate. As before the sphere is brought close to the corrugated plate and the separation distance is kept fixed. To measure the lateral Casimir force F^{lat} as a function of the phase φ, for a given sphere-plate separation, the corrugated plate is moved in the x direction in average steps of 0.46 nm using the x-piezo and the lateral Casimir force is measured at each step. As discussed above, correction voltages are applied to the z-piezo synchronous with the movement in the x direction to correct for any tilts from the mounting of the corrugated plate away from the vertical (x axis). This is repeated 60 times and the average lateral Casimir force at each step is recorded. The average lateral Casimir force measured is shown as the solid squares in Fig. 10. The scattered laser light leads to a small linear drift. Thus a corresponding straight line has been subtracted from the acquired data. The sinusoidal oscillations in the lateral Casimir force expected from Eq. (14) as a function of the phase difference between the two corrugations are clearly observed. The periodicity of the lateral Casimir force oscillation is also in agreement with the corrugation period of the plate. A sine curve fit to the observed data is shown as the solid line and corresponds to an amplitude of 3.2×10^{-13} N. From Eq. (14) this corresponds to a separation distance of $z=221\pm2$ nm between the two corrugated surfaces.

Here a more detailed error analysis is performed in comparison to Ref. [42]. The mean quadratic error of the average lateral force amplitude is $\sigma_{\bar{A}}=0.22\times10^{-13}$ N. The largest source of the systematic error is due to the resolution of the

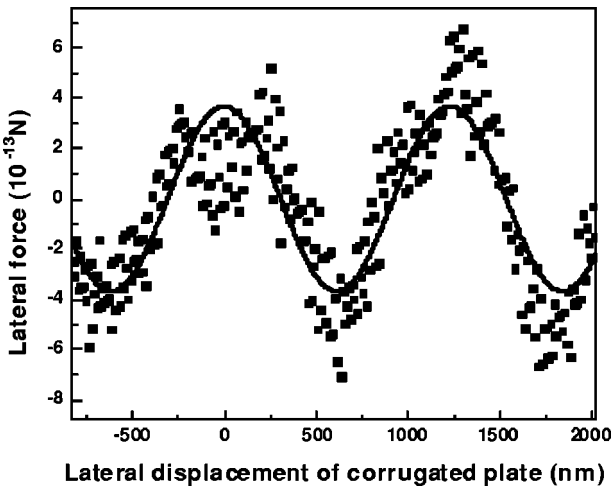

FIG. 10. The average measured lateral Casimir force as a function of the lateral displacement of the corrugated plate is shown as solid squares. The solid line is the best fit sine curve to the data leading to a lateral force amplitude of 3.2×10^{-13} N.

A/D board used in the data acquisition. This systematic error is $\Delta_A^{(s)}=0.33\times10^{-13}$ N. Using the value of Student coefficient $t_{0.95,60}=2$ one obtains for the half-width of the confidence interval, or for the total absolute error, $\Delta_A=\Delta_A^{(s)}+2\sigma_{\bar{A}}=0.77\times10^{-13}$ N with a 95% confidence probability. The resulting precision of the amplitude measurement at the closest point is around 24%.

The above lateral Casimir force measurement is repeated for other surface separations. First, the separation between the sphere and corrugated plate is increased by 12 nm with the z-piezo and the measurement is repeated. The average measured amplitude of lateral force is 2.6×10^{-13} N. Based on Eq. (14) this corresponds to $z=233\pm2$ nm consistent with the 12 nm increase in the separation distance. Thus the measured lateral Casimir force is in agreement with the complete theory taking into account the conductivity corrections. The separation distance is increased in 12 nm steps and the lateral Casimir force is measured for two more surface separations. The amplitudes of the measured forces 2.1×10^{-13} and 1.7×10^{-13} N were found to be consistent with the corresponding separation distances. In Fig. 11 a $\log_{10}$-$\log_{10}$ plot of the amplitudes of the measured lateral force as a function of the various separation distances is shown as solid squares. Here the separation distance of 221 nm determined from Fig. 10 is used for the closest point. The remainder of the points are fixed by the 12 nm step increase in the separation distance. A linear fit to the data yields a slope of 4.1 ± 0.2 consistent with the inverse fourth power z dependence of the lateral force expected from Eq. (14). Note that the corrections to this fourth power dependence are rather small given that the value $\beta<0.3$. Thus the lateral Casimir force demonstrates a very different dependence on separation distance than the lateral electrostatic force which leads to an inverse second power z dependence.

VI. LATERAL HYPOTHETICAL FORCES AND CONSTRAINTS ON THEIR PARAMETERS

The measurement of the lateral Casimir force presented in the above section gives the possibility of constraining the

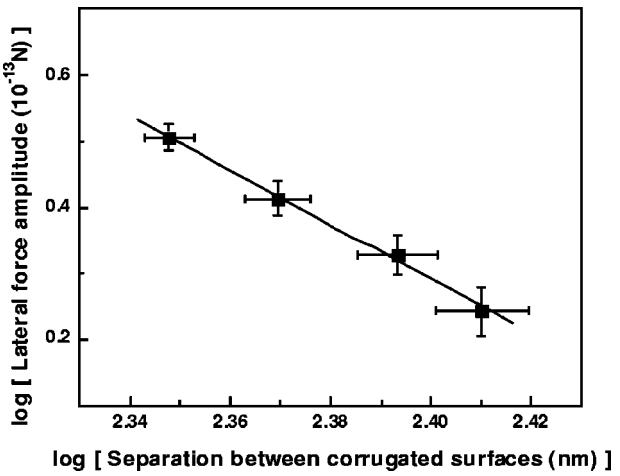

FIG. 11. The $\log_{10}$-$\log_{10}$ plot of the measured lateral Casimir force amplitude as a function of the surface separation distance is shown as solid squares. The slope of the straight line fit is 4.1 ± 0.2.

parameters of the hypothetical long-range interactions which may act between the test bodies. The problem of hypothetical long-range interactions has a long history. It is well known that such interactions complementary to the gravitational and electromagnetic forces are predicted by many extensions to the standard model [52]. They may be caused by the exchange of light elementary particles [3,25] or by extra-dimensional physics with a low compactification scale [53]. In both cases, additional Yukawa-type interactions are predicted that can be described by the potential

$$V^{Yu}(r) = -\frac{Gm_1m_2}{r}(1+\alpha_G e^{-r/\lambda}), \tag{23}$$

where G is the Newtonian gravitational constant, $m_{1,2}$ are the masses of the atoms, r is the separation distance between them, α_G is the dimensionless constant of hypothetical interaction, and λ is the interaction range.

It is common knowledge that at $\lambda > 10^{-4}$ m the gravitational experiments of Eötvos- and Cavendish-type lead to the strongest constraints on α_G [52]. However, for smaller λ the best constraints on α_G were obtained from the measurements of the normal Casimir force [26–31]. The above measurements of the lateral Casimir force deal with smaller forces than the previous experiments on the normal force. Thus they may lead to the competitive constraints on hypothetical interaction.

We start with the calculation of the lateral hypothetical Yukawa-type interaction for the configuration of a plate and a sphere with uniaxial corrugations. The same procedure as was used above for the Casimir force is applicable. The hypothetical interaction between two flat parallel plates of mass densities ρ and ρ' covered by a thin Au layer of density $\rho_{\rm Au}$ and thickness Δ can be obtained by an additive summation of the Yukawa parts of interatomic potentials (23). The result is [3,25–27,29,31]

$$E_{pp}^{Yu}(z) = -2\pi G\alpha_G\lambda^3 e^{-z/\lambda} \times[\rho_{\rm Au}-(\rho_{\rm Au}-\rho)e^{-\Delta/\lambda}][\rho_{\rm Au}-(\rho_{\rm Au}-\rho')e^{-\Delta/\lambda}]. \tag{24}$$

Note that in Sec. II, where the Casimir force was calculated, only the top metallic Au covering layers were essential and the underlying substances did not influence the force value.

The corrugations on both plates can be included by changing z in Eq. (24) for $z_2 - z_1$ defined in Eq. (7) and by averaging the obtained quantity over the corrugation period in accordance with Eq. (9). The result is given by

$$E_{pp}^{cor,Yu}(z,\varphi) = E_{pp}^{Yu}(z) I(\varphi), \tag{25}$$

where the notation is introduced

$$I(\varphi) \equiv \frac{1}{2\pi}\int_0^{2\pi} dt e^{-[b(\varphi)/\lambda]\cos(t-\alpha)}, \tag{26}$$

$b(\varphi)$ and α are defined in Eq. (8).

Using PFT from Eq. (12) and integrating the obtained force with respect to the separation distance, one finds the energy in the configuration of a corrugated plate and a sphere as

$$E^{Yu}(z,\varphi) = 2\pi R\lambda E_{pp}^{Yu}(z) I(\varphi) = 2\pi R\lambda E_{pp}^{cor,Yu}(z,\varphi). \tag{27}$$

Differentiating Eq. (27) with respect to a phase shift as it was done in Eq. (13) we come to the expression for the lateral hypothetical force for the configuration of a plate and a sphere covered with uniaxial corrugations

$$F^{lat,Yu}(z,\varphi) = -\frac{4\pi^2 R\lambda}{\Lambda} E_{pp}^{Yu}(z)\frac{dI(\varphi)}{d\varphi}. \tag{28}$$

The derivative with respect to φ can be calculated most easily if one uses the representation of the quantity I from Eq. (26) in the form of an infinite series

$$I(\varphi) = 1 + \sum_{n=1}^{\infty}\frac{a_n}{(2n)!}\left[\frac{b(\varphi)}{\lambda}\right]^{2n}, \tag{29}$$

where

$$a_n \equiv \frac{1}{2\pi}\int_0^{2\pi} dt(\cos t)^{2n}. \tag{30}$$

Differentiating Eq. (29) with respect to φ along with the use of Eq. (30) and substituting into Eq. (28) one finally obtains the lateral hypothetical force in the form

$$F^{lat,Yu}(z,\varphi) = -4\pi^2 R E_{pp}^{Yu}(z)\frac{A_1A_2}{\Lambda b(\varphi)}\sin\varphi \times\sum_{n=1}^{\infty}\frac{a_n}{(2n-1)!}\left[\frac{b(\varphi)}{\lambda}\right]^{2n-1}, \tag{31}$$

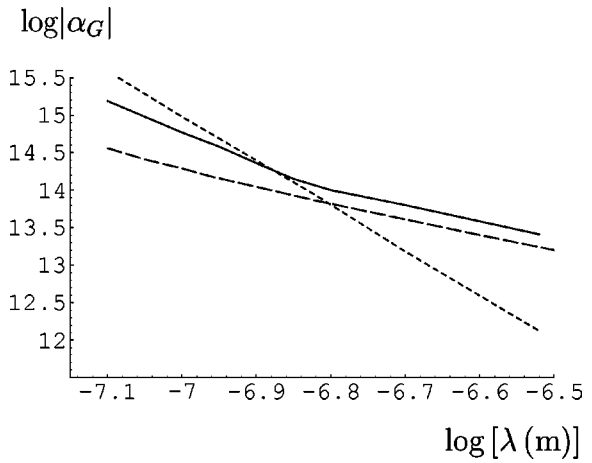

FIG. 12. Constraints on the Yukawa-type hypothetical interactions following from the measurement of the lateral Casimir force between corrugated surfaces (solid curve), normal Casimir force between a gold plate and a sphere (long-dashed curve), and normal Casimir force between dielectrics (short-dashed curve). The logarithm is to the base 10.

where $E_{pp}^{Yu}(z)$ is defined in Eq. (24). Notice that the coefficients a_n from Eq. (30) are simply calculated (e.g., $a_1=0.5$, $a_2=0.375$, $a_3=0.3125$, etc.) and the sum converges rapidly due to the factorial terms.

Now we are in a position to find the constraints on the hypothetical interactions following from the measurements of the lateral Casimir force. They can be obtained from the inequality

$$|F_{max}^{lat,Yu}|<\Delta_A, \tag{32}$$

where $\Delta_A=0.77\times10^{-13}$ N is the total absolute error of the lateral Casimir force measurements with a 95% confidence probability (see Sec. V). The quantity $F_{max}^{lat,Yu}$ is the maximal value of the lateral hypothetical force from Eq. (31) with respect to a phase shift φ computed at a smallest separation distance $z=221$ nm (note that the lateral Newtonian force is many orders less than Δ_A). The obtained constraints are plotted in Fig. 12 by the solid curve. The region of the (λ,α_G)-plane above the curve is prohibited, and below the curve is permitted by the results of the measurement of the lateral Casimir force. λ is measured in meters and the logarithm to the base 10 is used. The short-dashed curve in Fig. 12 was obtained from the old Casimir force measurements between dielectrics (see [3,25]). The long-dashed curve follows [31] from the measurements of the normal Casimir force between gold surfaces by means of atomic force microscope [10]. It is seen that in the interaction range 80 nm $<\lambda<150$ nm the constraints obtained by means of the lateral Casimir force measurements are of almost the same strength as the previous results. They, however, can be considered as more reliable as in the Casimir force measurements between dielectrics the measurement error was estimated rather approximately, whereas in Refs. [10,31] the confidence level and confidence probability were not indicated.

VII. CONCLUSIONS AND DISCUSSION

In the above, the experimental and theoretical investigation of the lateral Casimir force is presented. The lateral Casimir force was first demonstrated in Ref. [42]. Here the measurements were performed with the use of an AFM specially adapted to increase the sensitivity for detection of the lateral Casimir forces. The measured lateral force has the periodic dependence on the phase shift between the corrugations on both test bodies. The period of the lateral force coincides with the period of corrugations. The amplitude of the lateral force was found to be equal to 3.2×10^{-13} N at the separation distance 221 nm. The resulting experimental relative error of the amplitude measurement is 24% with a 95% confidence probability.

The normal electrostatic force between a sphere and a plate was used for both calibration of the cantilever and for the measurement of the residual potentials between the test bodies. The lateral electrostatic force leading to the inverse second power distance dependence is applied for the independent measurement of surface separation for the first time. The inverse fourth power dependence of the lateral Casimir force on separation distance was confirmed with high precision.

The experimental data were compared with a complete theory taking into account both finite conductivity and roughness corrections to the lateral Casimir force (the temperature corrections are not important at separations smaller than 0.5 μm). The finite conductivity corrections to the lateral Casimir force decrease the result computed for ideal metals by 30%–40% in the separation range under consideration. Thus the inclusion of these corrections is necessary for the comparison of theory and experiment.

The obtained experimental data on the lateral Casimir force were used to set constraints on the constants of Yukawa-type hypothetical interactions. In the interaction range 80 nm$<\lambda<$150 nm the obtained constraints are shown to be quite competitive (although a bit weaker) with the previously known ones from the measurement of the normal Casimir force. In the future with the increased precision one may expect that stronger constraints on the parameters of hypothetical long-range interactions will be obtained from the measurements of the lateral Casimir force.

Another prospective application where the above results can be used is in nanotechnology. With device dimensions shrinking to hundreds and even to tens of nanometers the Casimir force becomes the leading force which determines its functioning. The existence of the lateral Casimir force in the case of corrugated surfaces gives the possibility to actuate both normal and lateral translations by means of the electromagnetic zero-point fluctuations. This opens new promising opportunities for the application of the Casimir effect in microelectromechanical systems.

ACKNOWLEDGMENTS

This work was supported by a National Science Foundation Nanoscale Exploratory Research Grant and the National Institute for Standards and Technology through a Precision Measurement Grant. G.L.K. and V.M.M. were also supported by CNPq.

[1] H.B.G. Casimir, Proc. K. Ned. Akad. Wet. **51**, 793 (1948).
[2] P.W. Milonni, *The Quantum Vacuum* (Academic Press, San Diego, 1994).
[3] V.M. Mostepanenko and N.N. Trunov, *The Casimir Effect and its Applications* (Clarendon Press, Oxford, 1997).
[4] K.A. Milton, *The Casimir Effect* (World Scientific, Singapore, 2001).
[5] S.K. Lamoreaux, Phys. Rev. Lett. **78**, 5 (1997).
[6] G. Bressi, G. Carugno, R. Onofrio, and G. Ruoso, Phys. Rev. Lett. **88**, 041804 (2002).
[7] U. Mohideen and A. Roy, Phys. Rev. Lett. **81**, 4549 (1998).
[8] G.L. Klimchitskaya, A. Roy, U. Mohideen, and V.M. Mostepanenko, Phys. Rev. A **60**, 3487 (1999).
[9] A. Roy, C.-Y. Lin, and U. Mohideen, Phys. Rev. D **60**, 111101(R) (1999).
[10] B.W. Harris, F. Chen, and U. Mohideen, Phys. Rev. A **62**, 052109 (2000).
[11] A. Roy and U. Mohideen, Phys. Rev. Lett. **82**, 4380 (1999).
[12] V.B. Bezerra, G.L. Klimchitskaya, and V.M. Mostepanenko, Phys. Rev. A **62**, 014102 (2000).
[13] A. Lambrecht and S. Reynaud, Eur. Phys. J. D **8**, 309 (2000).
[14] G.L. Klimchitskaya, U. Mohideen, and V.M. Mostepanenko, Phys. Rev. A **61**, 062107 (2000).
[15] M. Bordag, G.L. Klimchitskaya, and V.M. Mostepanenko, Int. J. Mod. Phys. A **10**, 2661 (1995).
[16] G.L. Klimchitskaya and Yu.V. Pavlov, Int. J. Mod. Phys. A **11**, 3723 (1996).
[17] V.B. Bezerra, G.L. Klimchitskaya, and C. Romero, Phys. Rev. A **61**, 022115 (2000).
[18] C. Genet, A. Lambrecht, and S. Reynaud, Phys. Rev. A **62**, 012110 (2000).
[19] M. Bordag, B. Geyer, G.L. Klimchitskaya, and V.M. Mostepanenko, Phys. Rev. Lett. **85**, 503 (2000).
[20] G.L. Klimchitskaya and V.M. Mostepanenko, Phys. Rev. A **63**, 062108 (2001).
[21] B. Geyer, G.L. Klimchitskaya, and V.M. Mostepanenko, Int. J. Mod. Phys. A **16**, 3291 (2001).
[22] V.B. Bezerra, G.L. Klimchitskaya, and C. Romero, Phys. Rev. A **65**, 012111 (2002).
[23] V.B. Bezerra, G.L. Klimchitskaya, and V.M. Mostepanenko, Phys. Rev. A **65**, 052113 (2002).
[24] B. Geyer, G.L. Klimchitskaya, and V.M. Mostepanenko, Phys. Rev. A **65**, 062109 (2002).
[25] M. Bordag, U. Mohideen, and V.M. Mostepanenko, Phys. Rep. **353**, 1 (2001).
[26] M. Bordag, B. Geyer, G.L. Klimchitskaya, and V.M. Mostepanenko, Phys. Rev. D **58**, 075003 (1998).
[27] M. Bordag, B. Geyer, G.L. Klimchitskaya, and V.M. Mostepanenko, Phys. Rev. D **60**, 055004 (1999).
[28] J.C. Long, H.W. Chan, and J.C. Price, Nucl. Phys. B **539**, 23 (1999).
[29] M. Bordag, B. Geyer, G.L. Klimchitskaya, and V.M. Mostepanenko, Phys. Rev. D **62**, 011701(R) (2000).
[30] V.M. Mostepanenko and M. Novello, Phys. Rev. D **63**, 115003 (2001).
[31] E. Fischbach, D.E. Krause, V.M. Mostepanenko, and M. Novello, Phys. Rev. D **64**, 075010 (2001).
[32] H.B. Chan, V.A. Aksyuk, R.N. Kleiman, D.J. Bishop, and F. Capasso, Science **291**, 1941 (2001).
[33] H.B. Chan, V.A. Aksyuk, R.N. Kleiman, D.J. Bishop, and F. Capasso, Phys. Rev. Lett. **87**, 211801 (2001).
[34] E. Buks and M.L. Roukes, Phys. Rev. B **63**, 033402 (2001).
[35] Yu.S. Barash, Izv. Vuzov. Ser. Radiofiz. **16**, 1086 (1973) [Sov. Radiophys. **16**, 945 (1973)].
[36] S.J. van Enk, Phys. Rev. A **52**, 2569 (1995).
[37] R. Golestanian and M. Kardar, Phys. Rev. Lett. **78**, 3421 (1997).
[38] R. Golestanian and M. Kardar, Phys. Rev. A **58**, 1713 (1998).
[39] T. Emig, A. Hanke, R. Golestanian, and M. Kardar, Phys. Rev. Lett. **87**, 260402 (2001).
[40] L.S. Levitov, Europhys. Lett. **8**, 499 (1989).
[41] J.S. Hoye and I. Brevik, Physica A **181**, 413 (1992).
[42] F. Chen, U. Mohideen, G.L. Klimchitskaya, and V.M. Mostepanenko, Phys. Rev. Lett. **88**, 101801 (2002).
[43] I.E. Dzyaloshinskii, E.M. Lifshitz, and L.P. Pitaevskii, Usp. Fiz. Nauk **73**, 381 (1961) [Sov. Phys. Usp. **4**, 153 (1961)].
[44] C.M. Hargreaves, Proc. K. Ned. Akad. Wet. **68**, 231 (1965).
[45] J. Schwinger, L.L. DeRaad, Jr., and K.A. Milton, Ann. Phys. (N.Y.) **115**, 1 (1978).
[46] V.M. Mostepanenko and N.N. Trunov, Yad. Fiz. **42**, 1297 (1985) [Sov. J. Nucl. Phys. **42**, 818 (1985)].
[47] V.B. Bezerra, G.L. Klimchitskaya, and C. Romero, Int. J. Mod. Phys. A **16**, 3103 (2001).
[48] J. Blocki, J. Randrup, W.J. Swiatecki, and C.F. Tsang, Ann. Phys. (N.Y.) **105**, 427 (1977).
[49] P. Johansson and P. Apell, Phys. Rev. B **56**, 4159 (1997).
[50] M. Schaden and L. Spruch, Phys. Rev. Lett. **84**, 459 (2000).
[51] F. Chen and U. Mohideen, Rev. Sci. Instrum. **72**, 3100 (2001).
[52] E. Fischbach and C.L. Talmadge, *The Search for Non-Newtonian Gravity* (Springer, New York, 1999).
[53] N. Arkani-Hamed, S. Dimopoulos, and G. Dvali, Phys. Rev. D **59**, 086004 (1999).